ISCI, Volume *23*

Supplemental Information

Three-Dimensional Hierarchical Porous Nanotubes Derived from Metal-Organic Frameworks for Highly Efficient Overall Water Splitting

Yang Wang, Shenlong Zhao, Yinlong Zhu, Ruosang Qiu, Thomas Gengenbach, Yue Liu, Lianhai Zu, Haiyan Mao, Huanting Wang, Jing Tang, Dongyuan Zhao, and Cordelia Selomulya

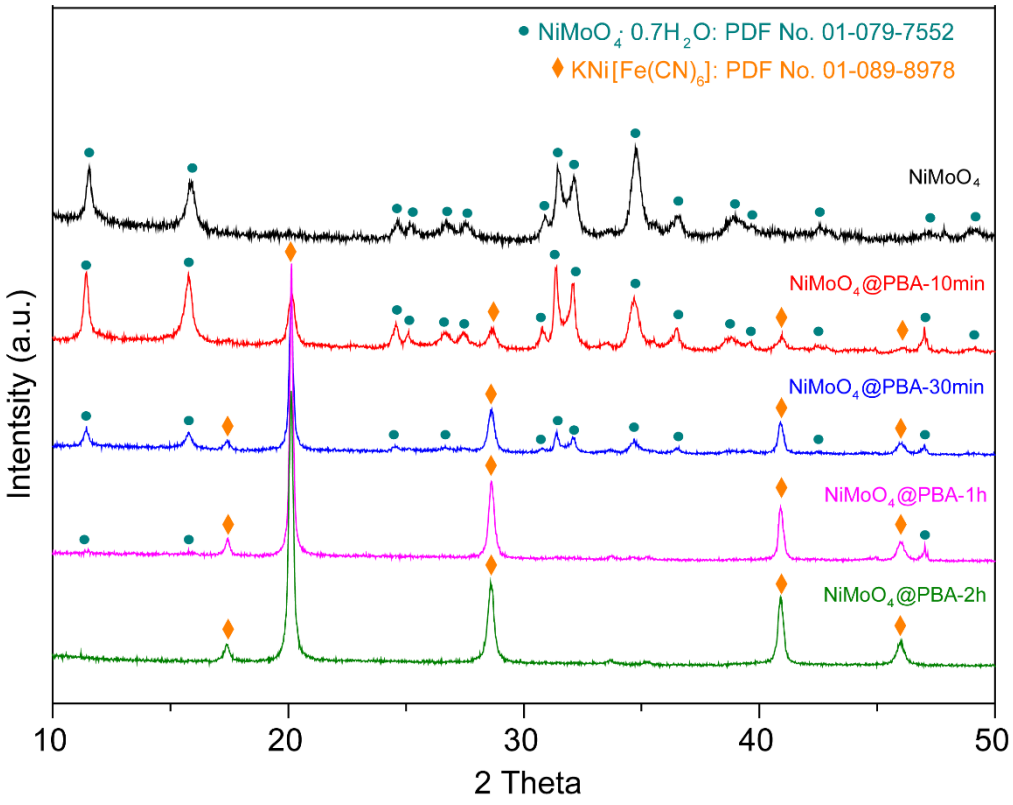

Figure S1. XRD patterns of $NiMoO_4$, $NiMoO_4$@PBA-10 min, $NiMoO_4$@PBA-30 min, $NiMoO_4$@PBA-1 h and $NiMoO_4$@PBA-2 h, related to **Figure 1**.

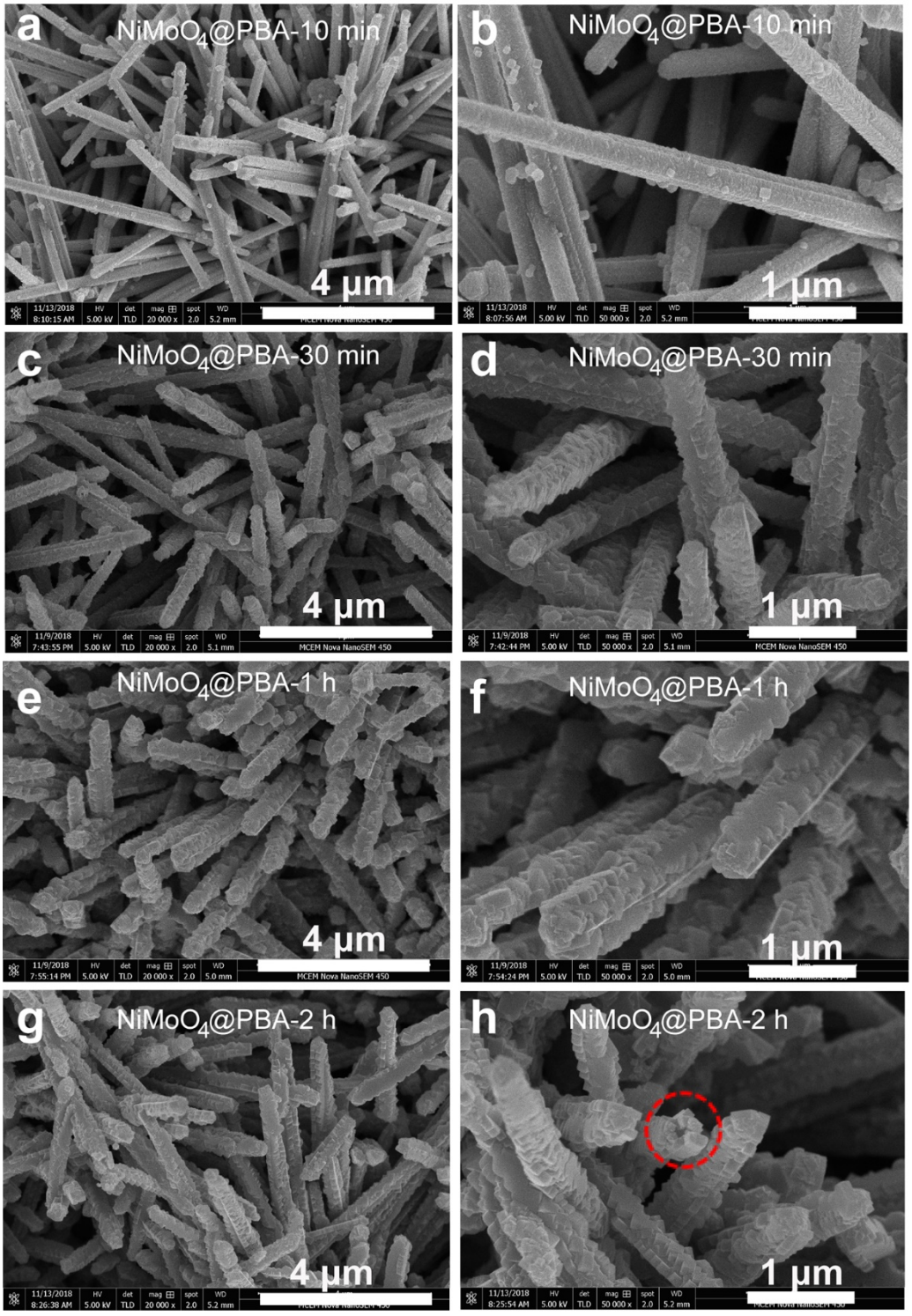

Figure S2. SEM images of $NiMoO_4$@PBA-10 min (a, b), $NiMoO_4$@PBA-30 min (c, d), $NiMoO_4$@PBA-1 h (e, f) and $NiMoO_4$@PBA-2 h (g, h) , related to **Figure 1**.

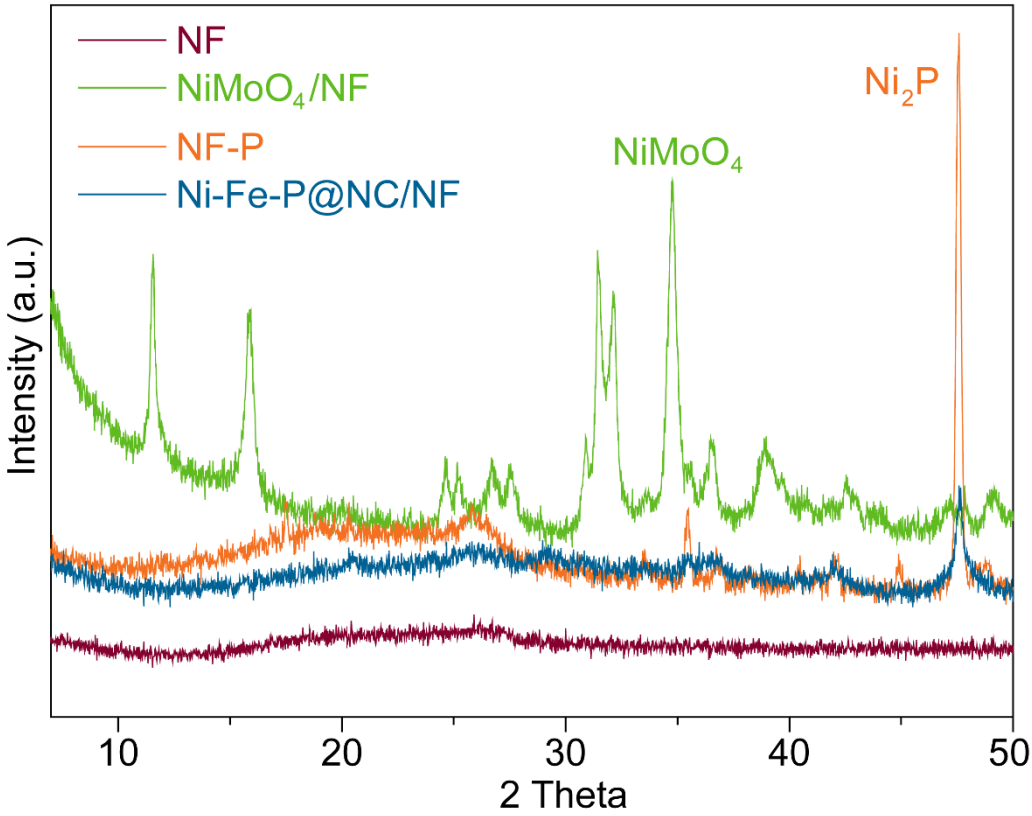

Figure S3. XRD patterns of Ni-Fe-P@NC/NF, $NiMoO_4$/NF, NF after phosphidation and original NF, related to **Figure 2**.

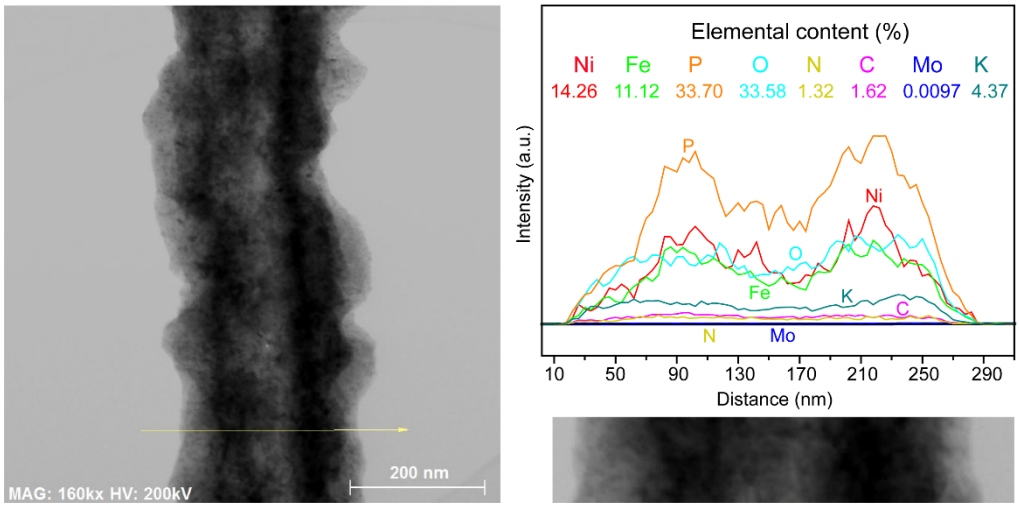

Figure S4. Line scan of Ni-Fe-P@NC nanotube and the elemental distribution on a radial direction, related to **Figure 2**.

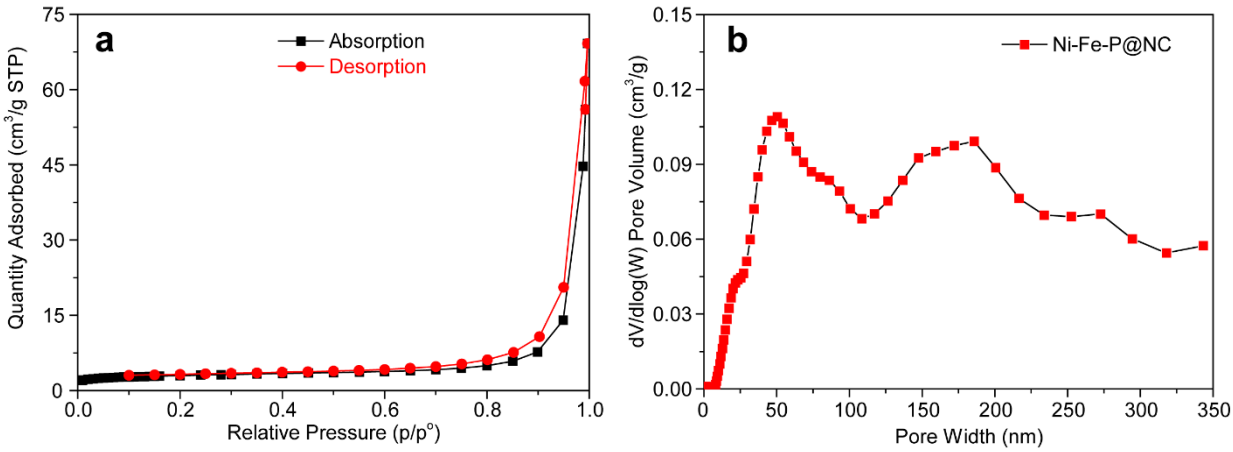

Figure S5. (**a**) N_2 adsorption-desorption isotherms and (**b**) corresponding pore size distribution plots of Ni-Fe-P@NC, related to **Figure 2**.

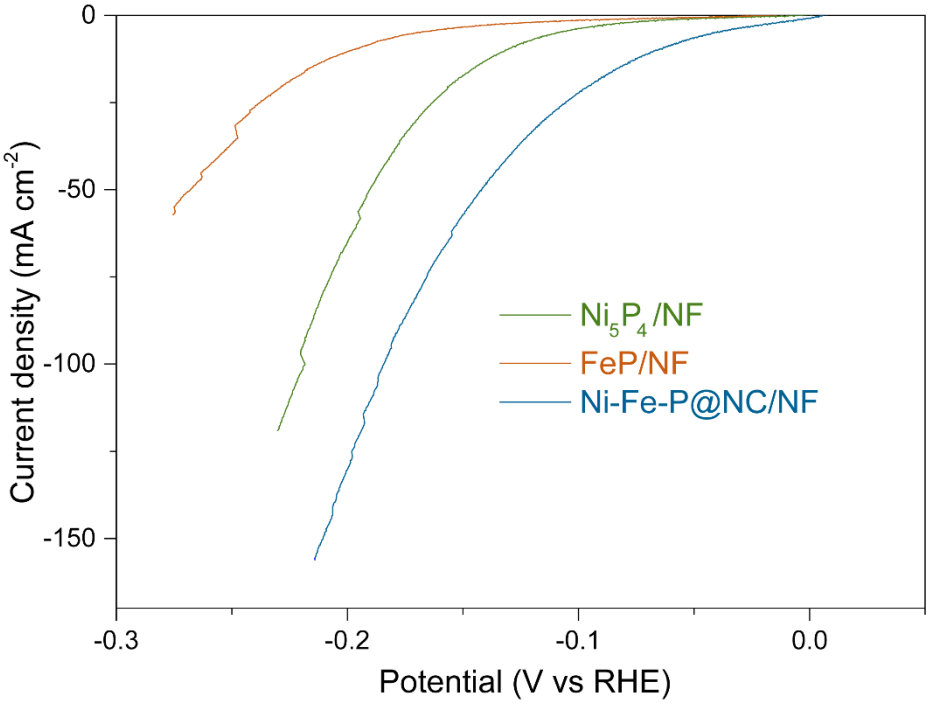

Figure S6. Linear sweep voltammetry (LSV) for HER comparison among Ni-Fe-P@NC/NF, Ni_5P_4 and FeP, related to **Figure 3**.

Faradaic efficiency

The Faradaic efficiency of hydrogen evolution reaction (FE_{HER}) was calculated based on the equation: $FE_{HER}= n_{H2} *2*F/ Q*100\%$

where n_{H2} was the amount of H_2 generated from HER, F was Faradaic constant and Q was the total charge applied on the working electrode.

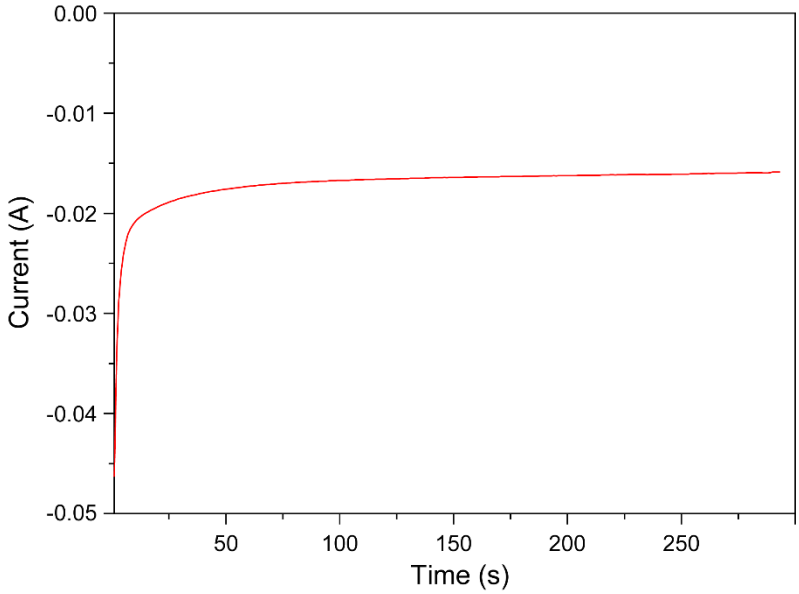

Figure S7. Chronoamperometric curves of Ni-Fe-P@NC/NF obtained at -0.1 V vs RHE for quantification of hydrogen, related to **Figure 3**.

When 5C of charge passed through the working electrode, the amount of obtained H_2 was detected by GC, which was 25.2 μmol. As there is systematic error including the relatively sealed electrochemical cell which might release H_2 during the transport to the GC, the error bar is around ± 3%.

$FE_{HER}= (25.2*10^{-6}$ mol*2*96485 C·mol$^{-1})$/5C*100%= 97.3% ± 3%

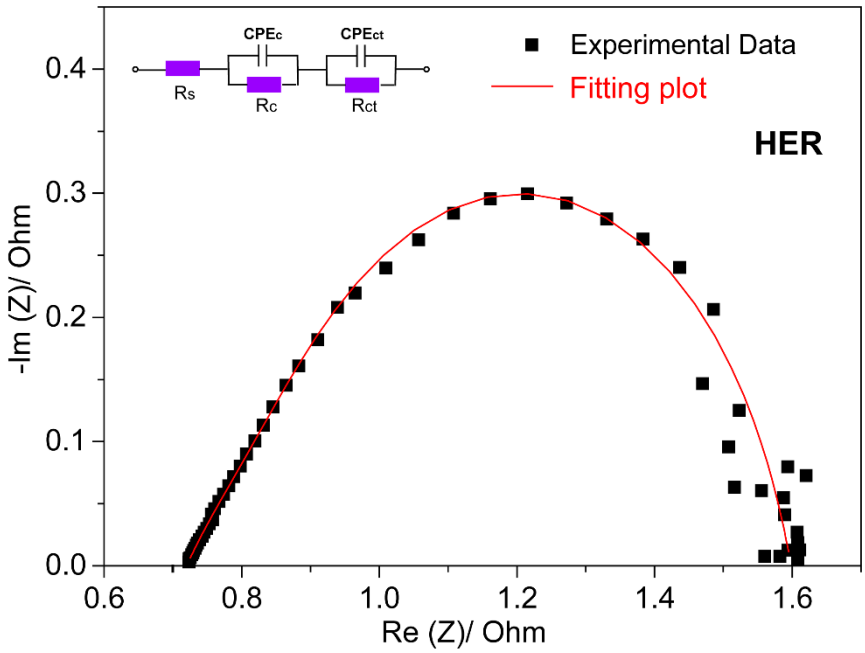

Figure S8. EIS Nyquist plots of Ni-Fe-P@NC/NF; inset: the corresponding equivalent circuit diagram, related to **Figure 3**.

R_s is the uncompensated solution resistance, CPE_c and R_c are the constant element and resistance reflecting electron transport at the interface between Ni-Fe-P@NC and NF, respectively. CPE_{ct} and R_{ct} are the constant phase element and charge transfer resistance at the Ni-Fe-P/electrolyte interface, respectively.

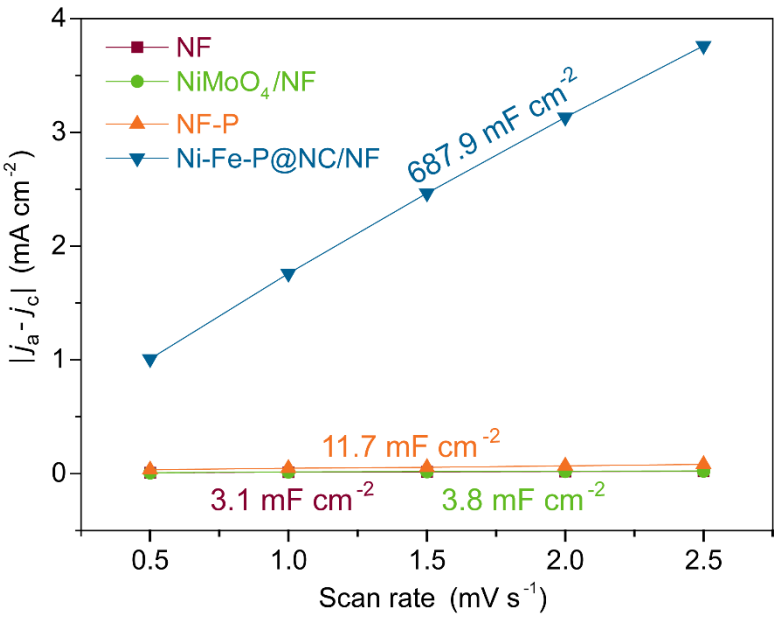

Figure S9. Plot showing the extraction of the double-layer capacitance (C_{dl}) for NF, $NiMoO_4$/NF, NF-P and Ni-Fe-P@NC/NF at -0.85 V *vs* Hg/HgO, related to **Figure 3**.

Normally, the specific capacitance for 1 cm^2 of a flat surface is around 20-60 $\mu F \cdot cm^{-2}$ and the average value of 40 $\mu F \cdot cm^{-2}$ is generally used for calculations. The specific capacitance can be obtained from geometric current density collected from the rectangular CV plots at a certain potential of -0.85 V *vs* Hg/HgO with a sweep rate from 0.5 to 2.5 mV s^{-1}.

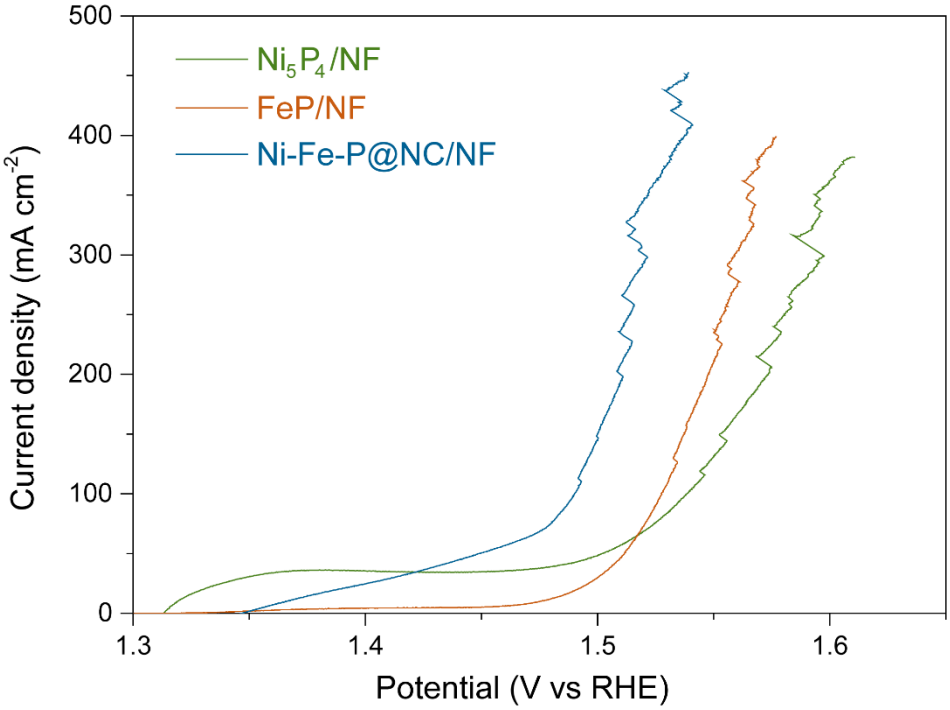

Figure S10. Linear sweep voltammetry (LSV) for OER comparison among Ni-Fe-P@NC/NF, Ni_5P_4 and FeP, related to **Figure 4**.

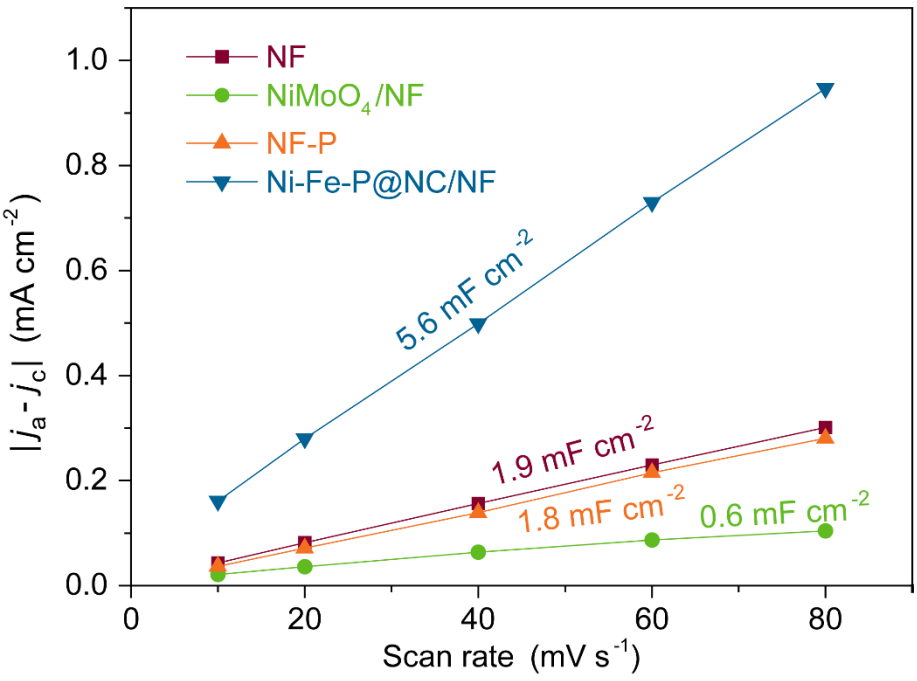

Figure S11. Plot showing the extraction of the double-layer capacitance (C_{dl}) for NF, $NiMoO_4$/NF, NF-P and Ni-Fe-P@NC/NF at 0.15 V *vs* Hg/HgO based on the CV curves at different scan rates with a potential range of 0.1~ 0.2 V *vs* Hg/HgO, related to **Figure 4**.

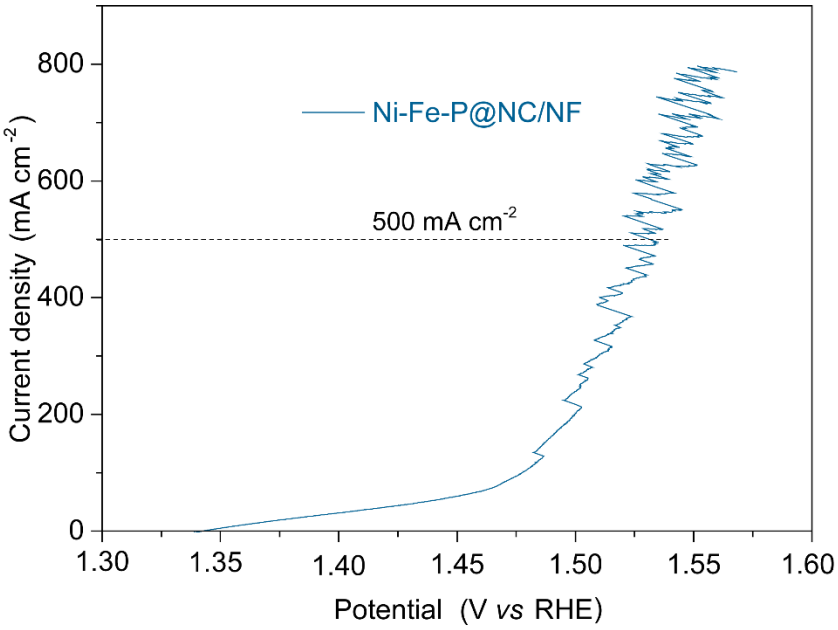

Figure S12. Linear sweep voltammetry (LSV) of Ni-Fe-P@NC/NF at higher potential LSV (500 mA cm^{-2} at 296 mV), related to **Figure 4**.

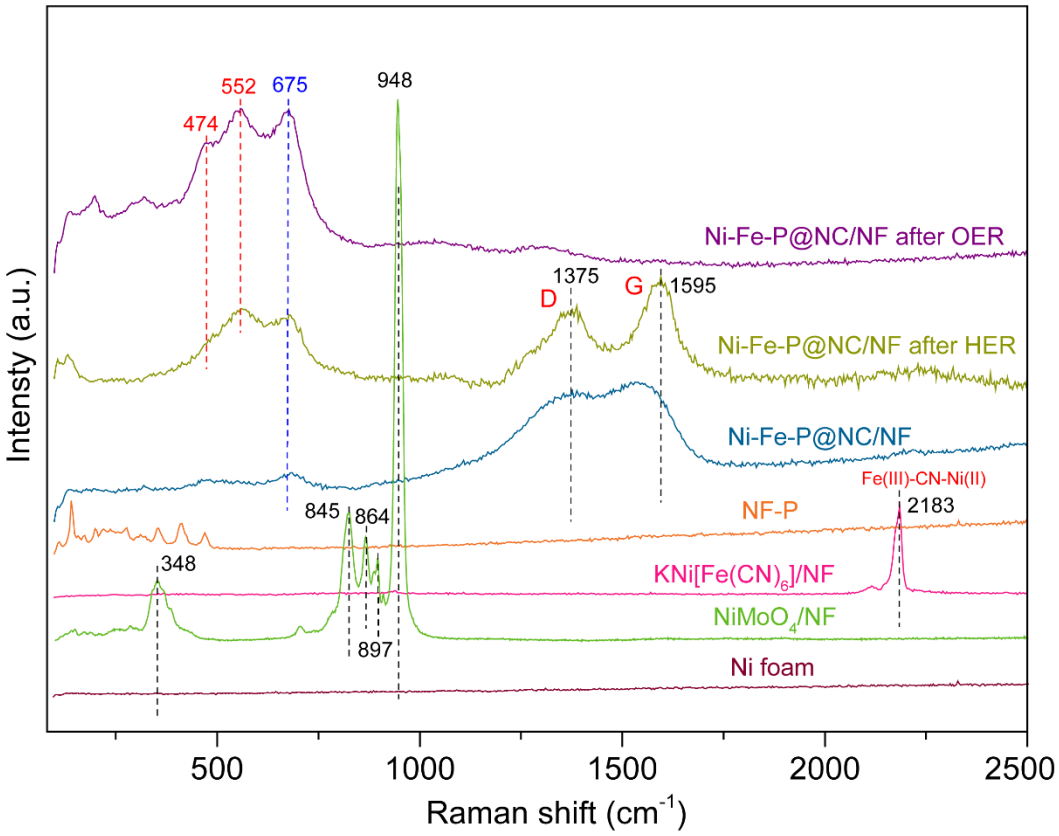

Figure S13. Raman spectra of Ni foam, $NiMoO_4$/NF, $KNi[Fe(CN)_6]$/NF, Ni-Fe-P@NC/NF, Ni-Fe-P@NC/NF after HER and Ni-Fe-P@NC/NF after OER, related to **Figure 2, 3 & 4**.

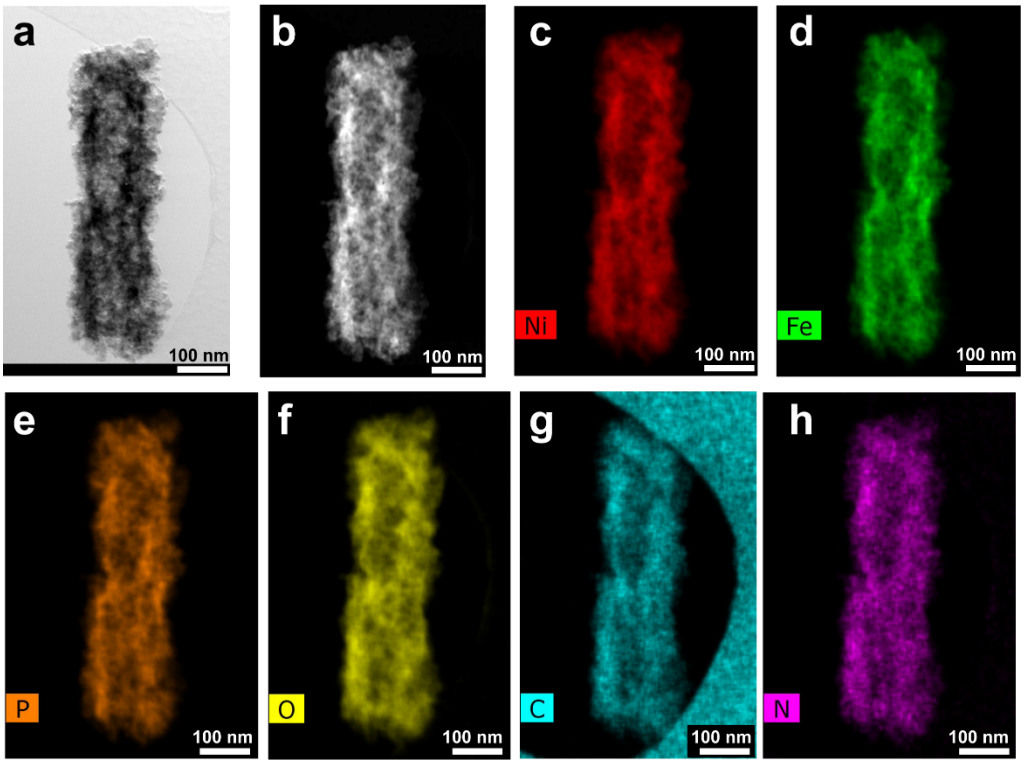

Figure S14. BF_DF (a), HAADF (b) and elemental mapping of each element (c-h) along the Ni-Fe-P@NC nanotube after HER at -50 mA cm^{-2} for 24 h. Scale bars are 100 nm, related to **Figure 3**.

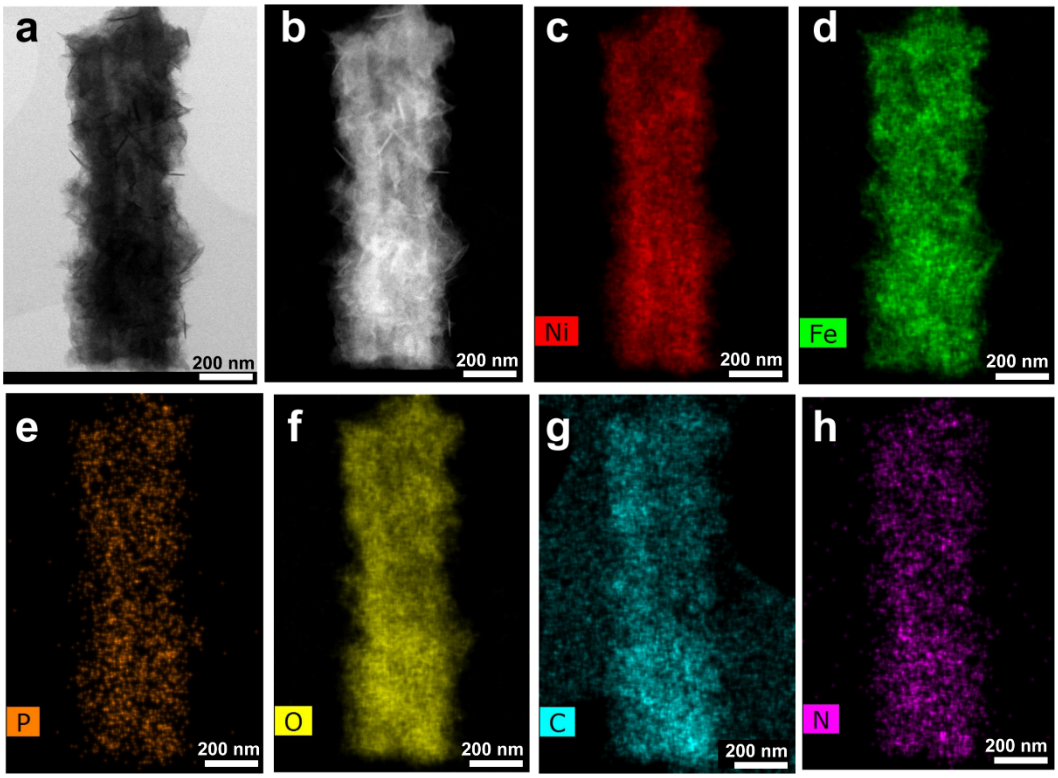

Figure S15. BF_DF (a), HAADF (b) and elemental mapping of each elements (c-h) along the Ni-Fe-P@NC nanotube after OER at 100 mA cm^{-2} for 24 h. Scale bars are 200 nm, related to **Figure 4**.

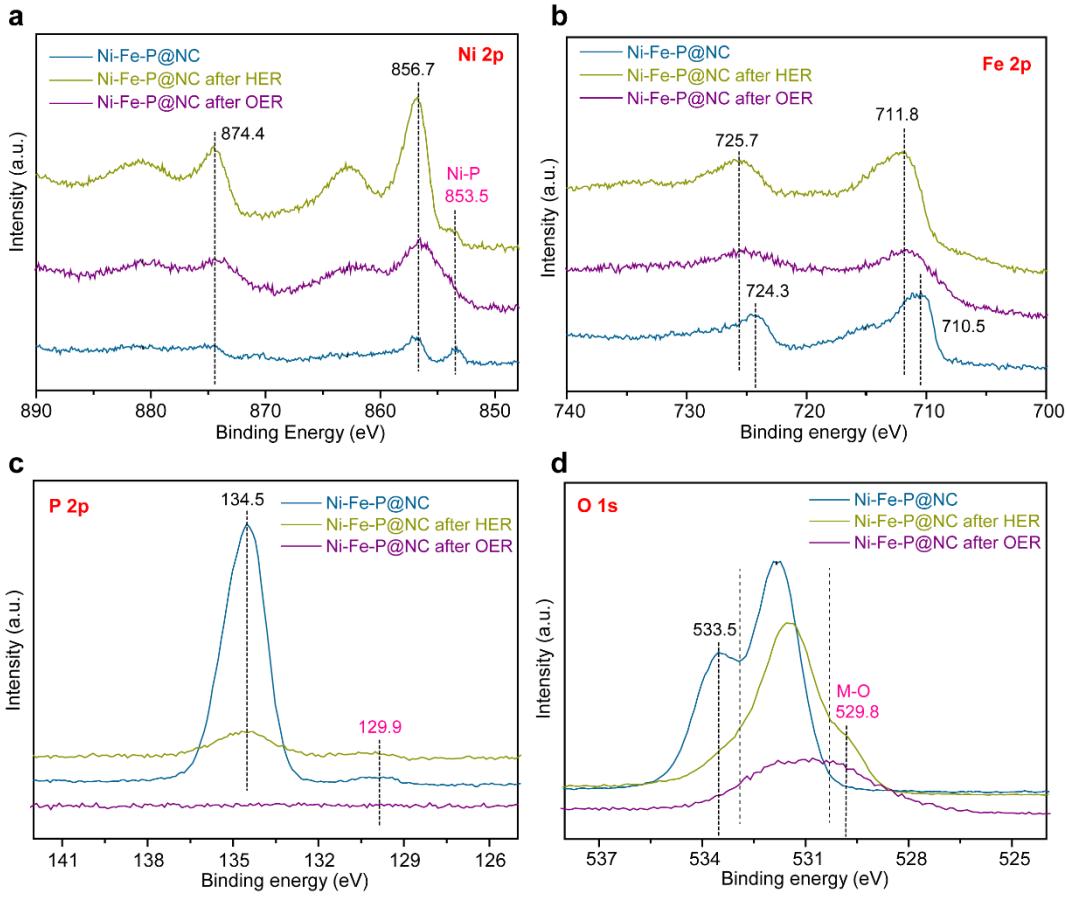

Figure S16. The XPS patterns of as-prepared Ni-Fe-P@NC sample, showing the signals of (a) Ni 2p, (b) Fe 2p, (c) P 2p and (d) O 1s, related to **Figure 2, 3 & 4**.

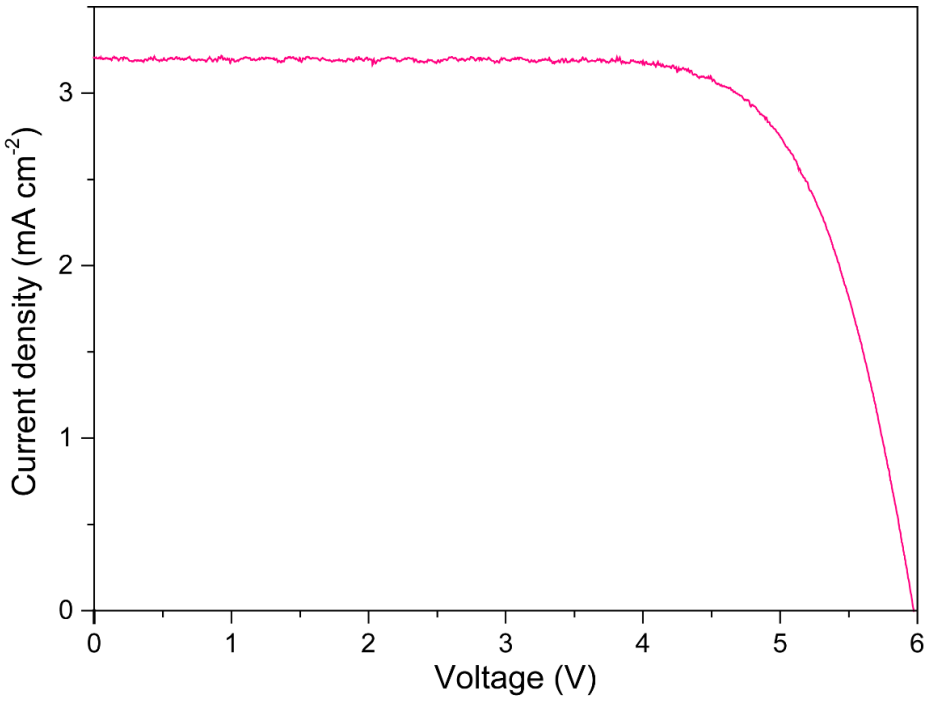

Figure S17. Current-voltage curve of a commercial silicon solar cell under simulated sunlight (1-sun illumination), related to **Figure 5**.

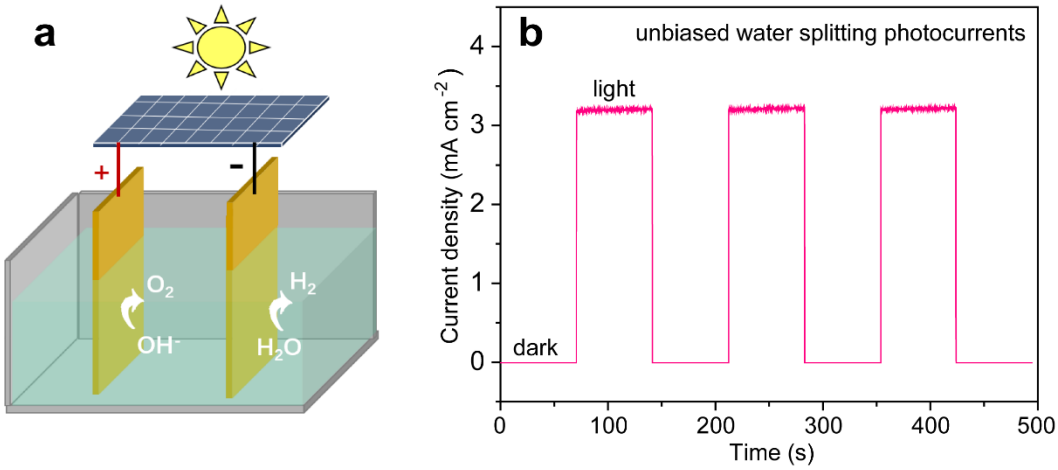

Figure S18. (a) Schematic diagram cell for photo water splitting. (b) Current density-time curve of the PV-EC device (1.0 M KOH) without external bias under chopped simulated AM 1.5 G 100 mW cm^{-2} illumination, related to **Figure 5**.

Table S1. ICP-MS result of Mo in Ni-Fe-P@NC, related to **Figure 1**.

Analyte	Mean Corrected Intensity	Calib. Conc. Units	Std. Dev.	Sample Conc. Units	Std. Dev.	RSD
Mo 202.031	2493.3	0.044 mg/L	0.0004	0.044 mg/L	0.0004	0.81%

As the concentration of the solution was 5 mg/L, the mass concentration of Mo in the solution or the sample was: w (Mo)= 0.044/5 = 0.88% which demonstrates the total conversion from $NiMoO_4$ to $KNiFe(CN)_6$.

Table S2. Values of elements circuit (**Fig. S8**) resulted from fitting the EIS data at -0.2 V *vs* RHE, related to **Figure 3**.

R_s (Ω)	Q_c ($F \cdot s^{(a-1)}$)	a_c	R_c	Q_{ct} ($F \cdot s^{(a-1)}$)	n_{ct}	R_{ct} (Ω)
0.7201	0.4107	0.5521	0.1093	0.2093	0.8502	0.6887

Table S3. Comparison of HER activity for Ni-Fe-P@NC/NF and well-known Ni/Fe-based catalysts in 1.0 M KOH, related to **Figure 3**.

Catalysts	Substrate	η @ -10 mA cm^{-2} (mV)	Tafel slope (mV dec^{-1})	References
Ni-Fe-P@NC	**Ni foam**	**65**	**81.0**	**This work**
$Ni_2P@FePO_x$	Ni foam	75	67	*Chem. Sci.,* **2018**, 9, 1375
NiFe NTAs	Ni foam	181	147.0	*ACS Appl. Energy Mater.* **2018**, 1, 3, 1210-1217
Ni/NiFe (oxy)hydroxide	Ni foam	210	71	*ACS Appl. Mater. Interfaces* **2018**, 10, 8585−8593
$FePO_4$ NW	Ni foam	42.7	104.5	*Adv. Mater.* **2017**, 29, 1704574
Mesoporous FeS_2[b]	Ni foam	96	78	*J. Am. Chem. Soc.* **2017**, 139, 13604
NiS_2/CoS_2-O NW	CFP	174	45	*Adv. Mater.* **2017**, 29, 1704681
MoS_2/ $Fe_5Ni_4S_8$	FeNi foam	120	45.1	*Adv. Mater.* **2018**, 30, 1803151
2D NiS_2	Ni foam	122	86	*Nano Energy* **2017**, 41, 148
V-doped NiS_2	Glass carbon	110	90	*ACS Nano* **2017**, 11, 11574
NiFe/$NiCo_2O_4$	Ni foam	105	88	*Adv. Funct. Mater.* **2016**, 26, 3515
$Ni_{0.33}Co_{0.67}S_2$ NW	Ti foil	88	118	*Adv. Energy Mater.* **2015**, *5*, 1402031
$Ni_{0.89}Co_{0.11}Se_2$ MNS	Ni foam	85	52	*Adv. Mater.* **2017**, 29, 1606521
Fe-Ni_3S_2/NF	Ni foam	47	95	*ACS Catal.* **2018**, 8, 5431−5441
$Ni_{0.33}Co_{0.67}Se_2$	CFP	106	60	*Adv. Energy Mater.,* **2017**, 7, 1602089
V-doped NiS_2	Glass carbon	110	90	*ACS Nano* **2017**, 11, 11574
NF@Ni/C-600	Ni foam	37	57	*Energy Environ. Sci.,* ***2018****,11, 2363-2371*
$Ni_{0.89}Co_{0.11}Se_2$ MNS	Ni foam	85	52	*Adv. Mater.* **2017**, 29, 1606521
$Ni_{0.33}Co_{0.67}Se_2$	CFP	65	35	*Adv. Energy Mater.,* **2017**, **7**, 1602089
$Ni_{0.8}Co_{0.1}Fe_{0.1}O_xH_y$	Ni foam	85	84.5	*ACS Catal.* **2018**, 8, 5621−5629
Ni_3FeN/r-GO	Ni foam	94	90	*ACS Nano* **2018**, 12, 245−253
Ni@NC-800	Ni foam	70	160	*Adv. Mater.* **2017**, 29, 1605957

Note: NT, Nanotube; NTAs, Nanotube Arrays; NW, Nanowire; MNS, Mesoporous nanosheet; NS, Nanosheet; CFP, Carbon fiber paper. [a]: N. A.=Not available.

Table S4. Comparison of OER activity for Ni-Fe-P@NC/NF and well-known Ni/Fe-based catalysts in 1.0 M KOH, related to **Figure 4**.

Catalysts	Substrate	η @ 10 mA cm^{-2} (mV)	η @ 50 mA cm^{-2} (mV)	η @ 100 mA cm^{-2} (mV)	Tafel slope (mV dec^{-1})	References
Ni-Fe-P@NC	**Ni foam**	**140**	**220**	**260**	**84.6**	**This work**
$Fe(PO_3)_2/Ni_2P$	Ni foam	177	N.A.	N.A.	51.9	*PNAS,* **2017**, 114,5607-5611
$Ni_3Fe_{0.5}V_{0.5}$	CFP	200	N.A.	264	39	*Nat. Comm.,* **2018**, 9, 2885
Fe-Ni@NC-CNTs	Ni foam	202	N.A.	N.A.	45.5	*Angew. Chem.* **2018**, 130, 9059 –9064
MoS_2/ $Fe_5Ni_4S_8$	FeNi foam	204	N.A.	N.A.	28.1	*Adv. Mater.* **2018**, 30, 1803151
$Ni_2P@FePO_x$	Ni foam	205	N.A.	230	32	*Chem. Sci.,* **2018**, 9, 1375
Fe-Ni_3S_2/NF	Ni foam	214	N.A.	249	42	*ACS Catal.* **2018**, 8, 5431−5441
$FePO_4$ NW	Ni foam	218	N.A.	N.A.	42.72	*Adv. Mater.* **2017**, 29, 1704574
Ni:Pi-Fe	Ni foam	220	N.A.	N.A.	37	*Chem. Mater.* **2016**, 28, 5659−5666
Ni(OH)2−CeO2	Carbon paper	220	N.A.	N.A.	81.9	*ACS Nano* **2018**, 12, 6245−6251
NiS_2/CoS_2-O NW	CFP	235	N.A.	N.A.	31	*Adv. Mater.* **2017**, 29, 1704681
$Ni_{0.8}Co_{0.1}Fe_{0.1}O_xH_y$	Ni foam	239	288	N.A.	45.4	*ACS Catal.* **2018**, 8, 5621−5629
NiFe-MOF	Ni foam	240	N.A.	N.A.	34	*Nat. Commun.* **2017**, 8, 15341
Ni_1Fe_2-O	GCE	244	N.A.	N.A.	39	*Adv. Energy Mater.* **2018**, 8, 1701347
NF@Ni/C-600	Ni foam	265	353	N.A.	54	*Energy Environ. Sci.,* **2018**, 11, 2363-2371
Ni_3FeN/r-GO	Ni foam	270	298	N.A.	54	*ACS Nano* **2018**, 12, 245−253

Ni–Co–P HNBs	Ni foam	270	N.A.	N.A.	76	*Energy Environ. Sci.*, **2018,**11, 872-880
$Ni_2P_4O_{12}$	carbon cloth	270	N.A.	N.A.	207	*Adv. Mater.* **2018**, 30, 1705045
Ni@NC-800	Ni foam	280	N.A.	N.A.	45	*Adv. Mater.* **2017**, 29, 1605957
$Ni_{1-x}Fe_xPS_3$@ MXene	GC	282	N.A.	N.A.	36.5	*Adv. Energy Mater.* **2018**, 8, 1801127
V-doped NiS_2	Glass carbon	290	N.A.	N.A.	45	*ACS Nano* **2017**, 11, 11574

CFP: Carbon fiber paper; GCE: glassy carbon electrode

Table S5. Summary of overall-water-splitting performance in 1.0 M KOH of various state-of-the-art Ni/Fe based bifunctional electro-catalysts, related to **Figure 5**.

Bifunctional catalysts	Substrate	$E_{J=10}$ (V)	Durability (h)	References
Ni-Fe-P@NC	**NF**	**1.47**	**100**	**This work**
Ni_2P@$FePO_x$	Ni foam	1.51	100	*Chem. Sci., **2018**, 9, 1375*
$Fe_{0.09}Co_{0.13}$-$NiSe_2$ NS	CFC	1.52	30	*Adv. Mater.* **2018**, 30, 1802121
NiFe LDH/Cu NW	Cu foam	1.54	48	*Energy Environ. Sci.* **2017**, 10, 1820
$FePO_4$ NW	Ni foam	1.54	15	*Adv. Mater.* **2017**, 29, 1704574
Fe-Ni_3S_2/NF	Ni foam	1.54	10	*ACS Catal.* **2018**, 8, 5431−5441
NiFe-MOF	Ni foam	1.55	20	*Nat. Commun.* **2017**, 8, 15341
Holey NiCoP NS	Ni foam	1.56	6	*J. Am. Chem. Soc.* **2018**, 140, 5241
V-doped NiS_2	Ni foam	1.56	20	*ACS Nano* **2017**, 11, 1157
NC-NiCu-NiCuN	Ni foam	1.56	50	*Adv. Funct. Mater.* **2018**, 28, 1803278
NFN-MOF/NF[a]	Ni foam	1.56	30	Adv. Energy Mater. 2018, 8, 1801065
NiFeSP	Ni foam	1.58	20	*ACS Nano* **2017**, 11, 10303
IFONFs-45	Fe foil	1.58	8.3	*Nat. Commun.* **2018**, 9, 1809
$Ni_{0.8}Co_{0.1}Fe_{0.1}O_xH_y$	Ni foam	1.58	50	*ACS Catal.* **2018**, 8, 5621−5629

NiCoP films	Scrap copper wires	1.59	24	*Adv. Energy Mater.* **2018**, 1802615
$Ni_{0.75}Fe_{0.125}V_{0.125}$-LDHs	Ni foam	1.591	15	*Small* **2018**, 14, 1703257
Ni_3FeN/r-GO	Ni foam	1.60	100	ACS Nano 2018, 12, 245−253
Se-$(NiCo)S_x/(OH)_x$ NS	Ni foam	1.6	66	*Adv. Mater.* **2018**, 30, 1705538
Fe-CoP	Ti foil	1.6	40	*Adv. Mater.* **2017**, 29, 1602441
Ni@NC-800	Ni foam	1.6	50	*Adv. Mater.* **2017**, 29, 1605957
Ni-Co-P HNB	Ni foam	1.62	20	*Energy Environ. Sci.,* **2018**,11, 872
Ni_3Se_2/Co_9S_8	Exfoliated graphene foil	1.62	10	Nano Lett. **2017**, 17, 4202
Ni-P	CFP	1.63	100	*Adv. Funct. Mater.* **2016**, 26, 4067
$NiCo_2S_4$ NW	Ni foam	1.63	50	*Adv. Funct. Mater.* **2016**, 26, 4661
Ni_2P NP	Ni foam	1.63	10	*Energy Environ. Sci.* **2015**, 8, 2347
Ni_2Fe_1-O	Ni foam	1.64	10	*Adv. Energy Mater.* **2018**, 8, 1701347
$Ni_{1-x}Fe_xPS_3$@ MXene	Ni foam	1.65	50	*Adv. Energy Mater.* **2018**, 8, 1801127
FeS NS	Iron foam	1.65	50	*Chem* **2018**, 4, 1139
Hierarchical $NiCo_2O_4$	Ni foam	1.65	15	*Angew. Chem. Int. Ed*. **2016**, 55, 6290
Ni-$P(Ni_{11}(HPO_3)_8(OH)_6$	Ni foam	1.65	100	*Energy Environ. Sci.,* **2018**, 11, 1287
$Co_{0.85}Se$/NiFe-LDH	Exfoliated graphene foil	1.67	10	*Energy Environ. Sci.* **2016**, 9, 478
NiFe/$NiCo_2O_4$	Ni foam	1.67	10	*Adv. Funct. Mater.* **2016**, 26, 3515
Ni_5P_4	Ni foil	~1.69	N. A.	*Angew. Chem. Int. Ed.* **2015**, 54, 12361
NiSe	Ni foam	1.69	N.A.	*Adv. Energy Mater.* **2018**, 8, 1702704
NiFe LDH	Ni foam	1.70	10	*Science* **2014**, 345, 1593
$FeSe_2$	Ni foam	1.72	24	*Angew. Chem. Int. Ed.* **2017**, 56, 10506
NiS_2/CoS_2–O	CFP	~1.77	21	*Adv. Mater.* **2017**, 29, 1704681

[a]NFN: NH_2-MIL-88B(Fe_2Ni) MOF

Transparent Methods

Chemicals and synthesis: $NaMoO_4 \cdot 2H_2O$, $Ni(NO_3)_2 \cdot 6H_2O$, NaH_2PO_2, $K_3[Fe(CN)_6]$, $FeSO_4 \cdot 7H_2O$, glycerol, NH_4F, Pt/C, RuO_2 and Nafion 117 solution were purchased from Sigma Aldrich. KOH pellets were purchased from Merck KGaA. MilliQ water with a resistivity ≥ 18 MΩ was used to prepare all aqueous solutions. All the reagents were used without further purification.

Synthesis of $NiMoO_4$ and $NiMoO_4$@PBA-XX on nickel foam

$NiMoO_4$ nanowires were synthesized by a modified hydrothermal method. Firstly, 0.242 g of $NaMoO_4 \cdot 2H_2O$ (1.0 mmol) and 0.291 g of $Ni(NO_3)_2 \cdot 6H_2O$ (1.0 mmol) were mixed together with 33 ml of MilliQ water and stirred for 20 min to obtain a precursor solution. Meanwhile, Ni foam cut into 1.0*3.0 cm^2 was sonicated in 3.0 M HCl for 10 min and then put in the Teflon lined autoclave with the above-prepared solution. Then the autoclave was further placed in an oven at 150°C for 4 h. After the reaction, the green powder was grown on Ni foam (denote as $NiMoO_4$/NF), rinsed for 3 times with distilled water and ethanol and then oven-dried at 80°C.
The prepared $NiMoO_4$/NF was weighed before transferred into a 25 mL-via with 16 mL 8.0 mg/mL of freshly prepared $K_3[Fe(CN)_6]$ solutions. The via contained $NiMoO_4$/NF was put in the oven at 90°C for the different duration (*i.e.* 10, 30, 60 and 120 min) and obtained $NiMoO_4$@PBA-10 min/NF, $NiMoO_4$@PBA-30 min/NF, $NiMoO_4$@PBA-1h/NF and $NiMoO_4$@PBA-2h/NF.

Synthesis of Ni-Fe-P@NC nanotubes on nickel foam

In the process of phosphidation step, two quartz boats, with 0.5 g of NaH_2PO_2 in the left boat and a piece of $NiMoO_4$@PBA-2h/NF (1*1.5 cm^2) in the right one, were placed in a stream of nitrogen in the furnace at 350°C for 2 h, where NaH_2PO_2 acted as the phosphorous source (denoted as Ni-Fe-P@NC/NF) and the CN group in PBA served as the C and N sources.

Synthesis of Ni_5P_4 on nickel foam

According to the method reported by Ge and co-workers(Ge et al, 2018), $Ni(NO_3)_2 \cdot 6H_2O$ (1 mmol, 0.291 g), urea (5 mmol, 0.3 g) and NH_4F (2 mmol, 0.074 g) were dissolved in water (20 mL) to obtain the precursor solution. Then a piece of clean nickel foam (1.0*3.0 cm^2) was palced in a Teflon-lined stainless steel autoclave which was immensed in the precursor solution, followed by heating them at 90°C for 12 h in an electric oven. After rreation, the obtained $Ni(OH)_2$/NF was cut into 1.0*1.5 cm^2 and phosphidated at 350°C for 2 h.

Synthesis of FeP

Accordint to the literature (Wang et al, 2019), $FeSO_4 \cdot 7H_2O$ (0.24g) and glycerol (2.5 mL) were dissolved in water (60 mL) which were further stirred for 30 minutes. Then the obtained solution was transferred into Teflon-lined stainless steel autoclaves, followed by heating them at 110°C for 12 h in an electric oven. After heating, the autoclave was turned off and cooled down naturally to room temperature. Then the target products (α-FeOOH) were collected by centrifugation, followed by drying at 70°C for several hours.
The obtained α-FeOOH and NaH_2PO_2 were mixed together and placed in a quatz boat which was palced in the middle of the oven. The atomic ratio for Fe to P is 1:10. Subsequently, the sample was heated at 350°C for 120 min at a heating rate of 5 ℃ min^{-1} in a flow N_2 atmosphere, and then naturally cooled to the room temperature. The obtained products were washed and collected by centrifugation. Finally, the powders were dried at 60℃ for 12 h.

Material characterizations. Phase fractions were determined using X-ray diffraction (XRD) and the data of all the materials were collected with Co Kα radiation on a Bruker D8 Advance eco diffractometer with a Lynxeye XE energy discrimination position-sensitive detector.
The morphologies of as-prepared samples were characterized by Scanning electron microscopy (SEM) using an FEI Nova NanoSEM at 5 kV. Conventional transmission electron microscopy (TEM) was carried out using a Tecnai T20 Twin operated at 200 kV with samples made by evaporating a drop of dispersions of the sub-micron wires in butanol onto holey-carbon-coated Cu grids. A Tecnai F20 SuperTwin operating at 200 kV was used to obtain scanning transmission electron microscopy (STEM) images and energy-dispersive spectrum (EDS) maps. STEM and TEM employed the same sample preparation process.
The Raman measurements were performed on a Renishaw Invia Raman microscope fitted with 488 nm Modulaser triple line argon-ion laser and a Coherent Inc 633 nm (red) HeNe laser.

"100%" power delivery would correspond to about 1mW on a 1 μm diameter spot of the sample. Use 5-10% of the power is fairly common to reduce the chance of sample heating damage. X-ray photoelectron spectroscopy (XPS) analysis was performed using either an AXIS Nova or an AXIS Ultra spectrometer (Kratos Analytical Inc., Manchester, UK) with a monochromated Al Kα source using the standard aperture (analysis area: 0.3 mm × 0.7 mm).

Pre-treatments for ICP-MS test. PerkinElmer Optima 8300 was apllied for testing the content of Mo in Ni-Fe-P@NC. Standard solutions with a series of concentrations of 0.1, 1, 5 and 10 ppm were prepared and tested to obtain the standard curve. Then 1 mg of sample was weighed and placed in a beaker where 4 mL of aqua regia was added to dissolve the sample. The obtained solution was heated and concentrated to 500 μL and diluted to suitable concentrations such as 100 ppm or 200 ppm. Then solution was further diluted to 5 ppm for ICP-MS test.

***Electrochemical measurements*.** A three-electrode system was set up with Ni-Fe-P@NC/NF (1.0*1.0 cm^2) clipped by a platinum clip as the working electrode, a graphite rod and Hg/HgO as the counter electrode and the reference electrode, respectively, in 1.0 M KOH. To prepare Pt/C and RuO_2 electrode, 10 mg of Pt/C or RuO_2 powders with 1 mL of ethanol and 50 uL of Nafion 117 solution were placed in 1.5 mL vial and was then sonicated for 5 minutes. 300 μL of the obtained Pt/C or RuO_2 suspension were dropped on a piece of Ni foam with a mass loading size of 1.0*1.0 cm^2 and dried in the fume cupboard. The FeP electrode was fabricated by suspending 12 mg of FeP particles in 1 mL of ethonal with 60 μL of Nafion 117 solution by sonication. Then, 0.5 mL of suspension was dropped on the nickel foam (1.0*1.0 cm^2) and dried in the fume cupboard. The electrochemical catalytic activity of Ni-Fe-P@NC/NF in 1.0 M KOH was evaluated by the polarization curves from linear sweep voltammetry (LSV) with a scan rate of 5 mV s^{-1}. All the potential values presented in this work were *iR*-corrected (aiming to remove the ohmic potential drop; $C_{correction} = E_{measure} - iR$) and referenced to the hydrogen electrode (RHE) unless indicated otherwise. The Frequency range for Electrochemical Impedance Spectroscopy (EIS) is from 100 kHz to 10 mHz on SP 150 (BioLogic). For comparison, the same measurements were performed on NF, $NiMoO_4$/NF and NF-P. To study the solar-to-hydrogen conversion, Ni-Fe-P@NC/NF acted as both the anode and cathode in the two-electrode system which connected to a commercial planar silicon photovoltaic (Voc = 6.0 V) working as the power source (illumination by 100 mW cm^{-2} simulated sunlight (1.5 G) for solar-to-hydrogen generation without external bias (Chen et al, 2010; Cox et al, 2014; Kuang et al, 2016; Luo et al, 2014).

Supplemental References

Chen, Z., Jaramillo, T. F., Deutsch, T. G., Kleiman-Shwarsctein, A., Forman, A. J., Gaillard, N., Garland, R., Takanabe, K., Heske, C., Sunkara, M., McFarland, E. W., Domen, K., Miller, E. L., Turner, J. A. & Dinh, H. N. (2010) Accelerating materials development for photoelectrochemical hydrogen production: Standards for methods, definitions, and reporting protocols. *Journal of Materials Research*, 25(1), 3-16.

Cox, C. R., Lee, J. Z., Nocera, D. G. & Buonassisi, T. (2014) Ten-percent solar-to-fuel conversion with nonprecious materials. *Proceedings of the National Academy of Sciences*, 111(39), 14057-14061.

Ge, Y., Dong, P., Craig, S. R., Ajayan, P. M., Ye, M. & Shen, J. (2018) Transforming Nickel Hydroxide into 3D Prussian Blue Analogue Array to Obtain Ni2P/Fe2P for Efficient Hydrogen Evolution Reaction. *Advanced Energy Materials*, 8(21), 1800484.

Kuang, M., Han, P., Wang, Q., Li, J. & Zheng, G. (2016) CuCo Hybrid Oxides as Bifunctional Electrocatalyst for Efficient Water Splitting. *Advanced Functional Materials*, 26(46), 8555-8561.

Luo, J., Im, J.-H., Mayer, M. T., Schreier, M., Nazeeruddin, M. K., Park, N.-G., Tilley, S. D., Fan, H. J. & Grätzel, M. (2014) Water photolysis at 12.3% efficiency via perovskite photovoltaics and Earth-abundant catalysts. *Science*, 345(6204), 1593-1596.

Wang, F., Fang, B., Yu, X. & Feng, L. (2019) Coupling Ultrafine Pt Nanocrystals over the Fe2P Surface as a Robust Catalyst for Alcohol Fuel Electro-Oxidation. *ACS Applied Materials & Interfaces*, 11(9), 9496-9503.